J Biomol NMR (2010) 46:227–244
DOI 10.1007/s10858-010-9398-8

ARTICLE

$^{15}N^{H/D}$-SOLEXSY experiment for accurate measurement of amide solvent exchange rates: application to denatured drkN SH3

Veniamin Chevelkov · Yi Xue · D. Krishna Rao · Julie D. Forman-Kay · Nikolai R. Skrynnikov

Received: 12 December 2009 / Accepted: 3 February 2010 / Published online: 27 February 2010

Abstract Amide solvent exchange rates are regarded as a valuable source of information on structure/dynamics of unfolded (disordered) proteins. Proton-based saturation transfer experiments, normally used to measure solvent exchange, are known to meet some serious difficulties. The problems mainly arise from the need to (1) manipulate water magnetization and (2) discriminate between multiple magnetization transfer pathways that occur within the proton pool. Some of these issues are specific to unfolded proteins. For example, the compensation scheme used to cancel the Overhauser effect in the popular CLEANEX experiment is not designed for use with unfolded proteins. In this report we describe an alternative experimental strategy, where amide ^{15}N is used as a probe of solvent exchange. The experiment is performed in 50% H_2O–50% D_2O solvent and is based on the (HACACO)NH pulse sequence. The resulting spectral map is fully equivalent to the conventional HSQC. To fulfill its purpose, the experiment monitors the conversion of deuterated species, $^{15}N^{D}$, into protonated species, $^{15}N^{H}$, as effected by the solvent exchange. Conceptually, this experiment is similar to EXSY which prompted the name of $^{15}N^{H/D}$-SOLEXSY (SOLvent EXchange SpectroscopY). Of note, our experimental scheme, which relies on nitrogen rather than proton to monitor solvent exchange, is free of the complications described above. The developed pulse sequence was used to measure solvent exchange rates in the chemically denatured state of the drkN SH3 domain. The results were found to correlate well with the CLEANEX-PM data, $r = 0.97$, thus providing a measure of validation for both techniques. When the experimentally measured exchange rates are converted into protection factors, most of the values fall in the range 0.5–2, consistent with random-coil behavior. However, elevated values, ca. 5, are obtained for residues R38 and A39, as well as the side-chain indole of W36. This is surprising, given that high protection factors imply hydrogen bonding or hydrophobic burial not expected to occur in a chemically denatured state of a protein. We, therefore, hypothesized that elevated protection factors are an artefact arising from the calculation of the reference (random-coil) exchange rates. To confirm this hypothesis, we prepared samples of several short peptides derived from the sequence of the drkN SH3 domain; these samples were used to directly measure the reference exchange rates. The revised protection factors obtained in this manner proved to be close to 1.0. These results also have implications for the more compact unfolded state of

V. Chevelkov · Y. Xue · D. Krishna Rao · N. R. Skrynnikov (✉)
Department of Chemistry, Purdue University, 560 Oval Drive, West Lafayette, IN 47907-2084, USA
e-mail: nikolai@purdue.edu

J. D. Forman-Kay
Program in Molecular Structure and Function, Hospital for Sick Children, 555 University Avenue, Toronto, ON M5G 1X8, Canada

J. D. Forman-Kay
Department of Biochemistry, University of Toronto, 1 King's College Circle, Toronto, ON M5S 1A8, Canada

Present Address:
V. Chevelkov
Forschunginstitut für Molekulare Pharmakologie (FMP), Robert-Rössle-Str. 10, 13125 Berlin, Germany

Present Address:
D. Krishna Rao
Department of Biochemistry and Molecular Biology, University of Texas Medical Branch, 301 University Boulevard, Galveston, TX 77555-0647, USA

drkN SH3, which appears to be fully permeable to water as well, with no manifestations of hydrophobic burial.

Keywords Amide solvent exchange · Isotopic shift · Exchange spectroscopy · (HACACO)NH experiment · CLEANEX experiment · Drosophila *drk* N-terminal SH3 domain · Protection factors · Residual structure · Hydrophobic cluster

Introduction

Since the early days of protein NMR, hydrogen exchange has been a valuable source of structural and dynamic information (Hvidt and Nielsen 1966). In folded proteins, amide groups are typically well protected (e.g., locked into hydrogen bonds and buried). Occasionally, however, portions of the protein structure become unraveled (i.e., experience large dynamic fluctuations which are usually of local nature, but can also be cooperative). For a brief moment, amide sites become exposed to solvent and undergo proton exchange. The resulting two-step kinetic scheme was first analyzed by Linderstrøm-Lang (Linderstrøm-Lang 1955; Zheng et al. 1995).

Experimentally, solvent exchange in folded proteins can be conveniently studied by deuterium substitution. In a basic version of this experiment, a lyophilized protein is dissolved in D_2O and a series of 2D spectra is recorded to monitor the progressive loss of amide proton signals (Wagner and Wüthrich 1982). This technique is generally suited for detection of exchange in the time frame from minutes to months, which is typical for folded proteins. Proton–deuterium substitution can also be monitored in systems with fast exchange, which are mainly of interest in the context of protein (un)folding. Such applications require stop-flow type experiments (Roder et al. 1988). Recent ultrafast 2D experiments further expand the scope of these measurements (Gal et al. 2007).

While stop-flow measurements of non-equilibrium kinetics are of great interest, most of the fast exchange measurements are conducted using equilibrium techniques. In principle, direct observation of exchange cross-peaks between water and amides is possible in homonuclear EXSY (NOESY, ROESY) spectra (Dobson et al. 1986; Otting et al. 1991; Dötsch et al. 1995). These are, however, low-sensitivity experiments that are normally run in a 3D mode and, hence, this scheme found little use in the context of amide exchange measurements. Instead, a variety of saturation transfer schemes have been used toward this goal (Spera et al. 1991; Kriwacki et al. 1993; Dalvit and Hommel 1995; Hwang et al. 1998; Zhou and van Zijl 2006). In a basic version of the saturation transfer experiment, an HSQC sequence is used to monitor the loss of signal due to the exchange of amide protons with presaturated water protons. While this approach is simple and robust, it encounters a number of technical and conceptual difficulties. Several problems arise from the need to manipulate water magnetization: (1) water signal radiation damping can cause subtraction artefacts and false detection of solvent exchange; (2) water saturation requires very long recycling delays to restore water magnetization to a true equilibrium and thus obtain a proper reference spectrum; (3) instead of the decay/build-up pair, as recorded in the standard EXSY experiments, only the build-up profile is usually available; (4) the initial degree of saturation of the water signal and the recovery rate of water magnetization may need to be known for data analyses.

All of these issues can be successfully addressed, as demonstrated in many elegant experimental designs (Grzesiek and Bax 1993b; Mori et al. 1996; Hwang et al. 1998). However, there is another layer of complexity to this problem: the presence of several alternative magnetization transfer pathways makes it difficult to isolate and quantify amide exchange (van de Ven et al. 1988; Kriwacki et al. 1993; Otting and Liepinsh 1995). The potentially competing pathways include: (5) intramolecular NOE transfer between saturated $^1H^{\alpha}$ spins (resonances in the proximity of the water line) and $^1H^N$; (6) intramolecular TOCSY transfer between saturated $^1H^{\alpha}$ spins and $^1H^N$; (7) relayed transfer, where the saturation first propagates from water to hydroxyl and amine sites via chemical exchange and then onto $^1H^N$ spins via NOE; (8) intermolecular NOE transfer from water to $^1H^N$.

Likewise, many original experimental schemes have been developed to counter the unwanted propagation effects (5–8) (Gemmecker et al. 1993; Melacini et al. 1999; Jensen et al. 2007) In particular, the CLEANEX sequence is considered to be a benchmark experiment for accurate quantification of amide exchange, largely free of interferences (5–8) (Hwang et al. 1997, 1998). Briefly, in this experiment proton magnetization is locked at the effective angle of 35° to the direction of the static magnetic field, thus ensuring the cancelation of the Overhauser effect in the macromolecular limit (Griesinger and Ernst 1987). In what follows, we discuss this experiment in more detail and note, in particular, that its performance can be degraded in applications involving unfolded proteins.

In addition to various implementations of the saturation (inversion) transfer scheme, one can mention another class of experiments where heteronuclei (^{15}N or ^{13}C) are used as a probe for proton solvent exchange. In the early experiments by Hawkes et al. and Henry et al., ^{15}N and ^{13}CO lineshape variations due to modulation of isotopic shifts/coupling constants by proton–deuterium exchange have been exploited (Hawkes et al. 1978; Henry et al. 1987).

Exchange-induced modulation of scalar couplings can also be observed in the H_2O solvent (scalar relaxation of the first kind). This effect was recently exploited in studies of solvent exchange by Kateb et al. (2007). Generally these methods are well suited for studies of faster exchange rates, $k \geq 10\ s^{-1}$. Another approach is to use the decay of two-spin modes, H_xN_z or H_zN_z, to quantify the exchange rates (Henry and Sykes 1993; Skrynnikov and Ernst 1999). A limitation of this method, however, is that it is difficult to separate exchange from relaxation.

In this paper we introduce a (HACACO)NH-type (Shang et al. 1997; Hitchens et al. 1999) sequence that monitors the interconversion between proton- and deuterium-bound ^{15}N spins in 50% H_2O–50% D_2O solution. In a single experimental run we obtain both build-up and decay profiles, similar to a conventional EXSY experiment.[1] The build-up corresponds to conversion of the initially selected $^{15}N^{D}$ species into $^{15}N^{H}$. The decay, on the other hand, corresponds to the gradual loss of the selected $^{15}N^{H}$ population as a result of deuterium-for-proton substitution. The experiment is suitable for exchange rates in a range from ca. 0.2 to 20 s^{-1}, limited on one side by ^{15}N relaxation and on the other side by undesirable effects of fast exchange outside the mixing period.

Notably, our experimental scheme is free from complications associated with water signal (1–4) as well as extraneous transfer pathways (5–8). Indeed, during the mixing time the magnetization in our experiment is of the form N_z and the mixing occurs in a form of exchange between proton- and deuterium-bound ^{15}N spins. Under these conditions the system is oblivious to the state of the proton (deuterium) pool and to various transfer effects that occur among protons. It is the status of nitrogen that serves as a marker of exchange. These properties are especially valuable in studies of unfolded proteins where the performance of other experimental schemes can be called into question.

Experiment

The new pulse sequence is designed for use with 50% H_2O–50% D_2O solvent (other proportions can also be used, albeit at the expense of sensitivity). The scheme of the experiment is a variation of classical exchange spectroscopy theme (Jeener et al. 1979). First, the magnetization is delivered from $^{1}H^{\alpha}$ to ^{15}N. Then the two species, $^{15}N^{H}$ and $^{15}N^{D}$, are frequency-labeled during the evolution time t_1; the respective ^{15}N resonances are resolved due to the isotopic shift of ca. 0.7 ppm (Hansen 2000). This is followed by a variable-length mixing time period, τ_{mix}, during which $^{15}N^{H}$ moieties are partially transformed into $^{15}N^{D}$ and vice versa due to the exchange with solvent. Finally, the magnetization is transferred to $^{1}H^{N}$ for detection. The resulting spectral peaks represent:

(1) amide groups that are protonated during t_1, remain protonated after the mixing time τ_{mix}, and as such are detected during t_2.
(2) amide groups that are deuterated during t_1, become protonated during τ_{mix}, and as such are detected during t_2.

Clearly, in terms of the conventional exchange spectroscopy these two signals can be classified as an ‘axial peak’ and ‘cross peak’, respectively. When the intensities of these peaks are plotted as a function of τ_{mix}, the familiar decay and build-up profiles are obtained (Jeener et al. 1979). Standard analysis then yields the sought-for exchange rates. In recognition of the fundamental similarity with EXSY, we named the pulse sequence $^{15}N^{H/D}$-SOLEXSY (SOLvent EXchange SpectroscopY).

The actual sequence is shown in Fig. 1a and the coherence transfer steps are schematically indicated in Fig. 1b. The sequence borrows from the HA(CACO)N experiment (Wang et al. 1995; Kanelis et al. 2000) and the transfer scheme is generally equivalent to the one found in the (HACACO)NH (Shang et al. 1997; Hitchens et al. 1999). Initially, $^{1}H^{\alpha}$ magnetization is transformed into $N_xC_z^{'}$ coherence using standard polarization transfer steps (point c in Fig. 1). This coherence is built in all amide sites, irrespective of whether they are protonated or deuterated. This coherence is then refocused into N_x and, at the same time, the chemical shift of ^{15}N is recorded during the semi-constant-time period between points c and d (Grzesiek and Bax 1993a). At this point, the signals from the protonated and deuterated groups can be distinguished on the basis of the isotopic shift, $N_x(\omega_{NH}t_1)$ versus $N_x(\omega_{ND}t_1)$. The subsequent filtering element, $(1/2J_{NH}) - 90^{\circ}_{x}90^{\circ}_{\pm x}(^{1}H), 180^{\circ}_{x}(^{15}N) - (1/2J_{NH})$, inserted between points d and e introduces the sign coding: the magnetization from the protonated sites is encoded as $\pm N_x(\omega_{NH}t_1)$, whereas the magnetization from the deuterated sites remains invariant, $N_x(\omega_{ND}t_1)$. During the mixing time, point e to point f, some of the protonated species become deuterated and vice versa. Because HSQC-style detection is used in this sequence, only the protonated species are detected. Specifically, the protonated amides that remain protonated after τ_{mix} give rise to the observable $\pm H_x(\omega_{NH}t_1, \omega_H t_2)$, whereas the deuterated sites that become protonated during τ_{mix} give rise to $H_x(\omega_{ND}t_1, \omega_H t_2)$.

[1] Generally speaking, our experiment can be described as an EXSY-style counterpart to the lineshape analyses by Hawkes et al. and spin echo experiments by Kateb et al., extending the observation window toward the slower exchange rates. At the same time, there is clearly a parallel with ^{15}N zz-exchange experiment by Kay and co-workers (Farrow et al. 1994).

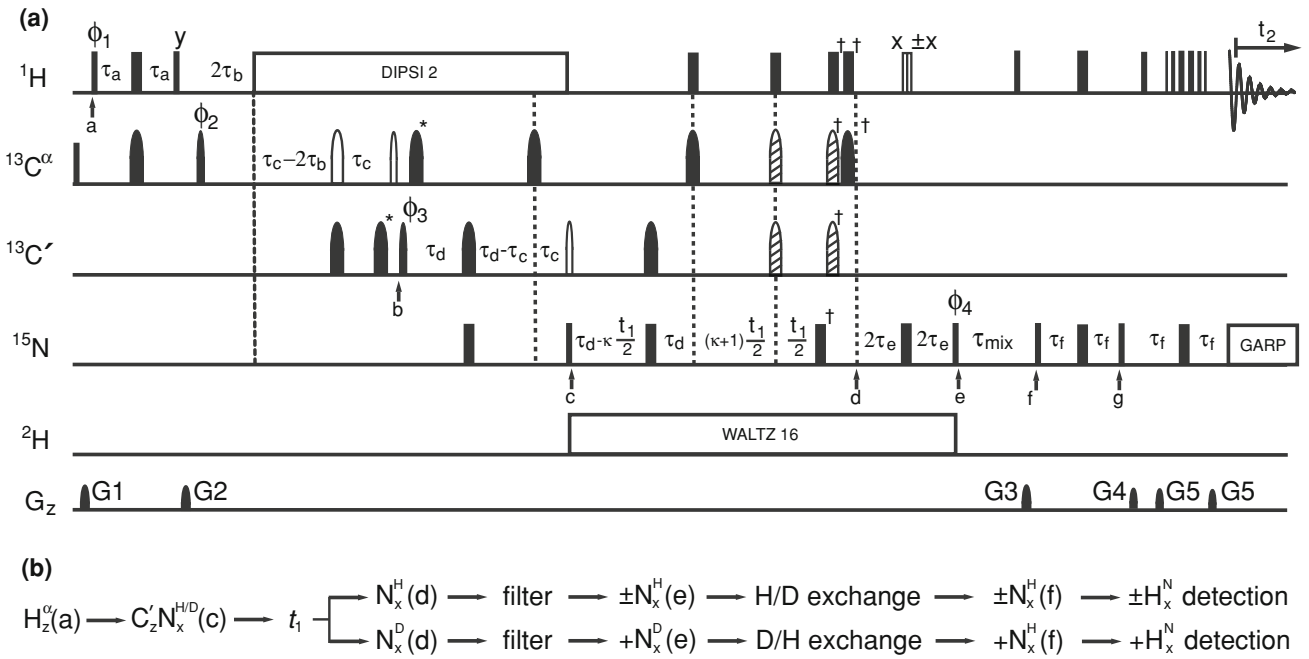

Fig. 1 $^{15}N^{H/D}$-SOLEXSY experiment for measuring solvent exchange rates by monitoring the magnetization transfer between proton- and deuterium-bound ^{15}N spins in 50% H_2O–50% D_2O solvent. **a** Pulse sequence (see Sect. "Materials and Methods" for experimental parameter settings). **b** Coherence transfer scheme

The selected regions of the HSQC-type spectral planes recorded with the pulse sequence Fig. 1a are illustrated in Fig. 2. To begin with, consider the case when $\tau_{mix} = 0.7$ ms. This mixing time is too short to build an appreciable $H_x(\omega_{ND}t_1, \omega_H t_2)$ term. The signal is, therefore, limited to $\pm H_x(\omega_{NH}t_1, \omega_H t_2)$ (Fig. 2, upper row, columns A and B). When the duration of the mixing time is increased, the intensity of $\pm H_x(\omega_{NH}t_1, \omega_H t_2)$ signals drops due to the partial displacement of amide protons by deuterons. At the same time, the intensity of $H_x(\omega_{ND}t_1, \omega_H t_2)$ signals increases as some of the initially deuterated amides become protonated. As a result, for sufficiently long mixing times the two components are equalized. This is demonstrated in the bottom row of Fig. 2, columns A and B, where the peaks representing $\pm H_x(\omega_{NH}t_1, \omega_H t_2)$ (116.5 ppm nitrogen chemical shift) have roughly the same intensity as $H_x(\omega_{ND}t_1, \omega_H t_2)$ (115.8 ppm).

The sign coding of the proton component allows for separation of the signals into two sub-spectra (Xu et al. 2005). Addition of spectra A and B eliminates the 'axial peaks' $H_x(\omega_{NH}t_1, \omega_H t_2)$. Conversely, subtraction of A and B leads to cancelation of the 'cross peaks' $H_x(\omega_{ND}t_1, \omega_H t_2)$. This approach avoids crowding of the spectra, ensuring that the total number of peaks is the same as in the conventional HSQC map (especially important for applications involving unfolded proteins). The spectra processed in this fashion are presented in the right part of Fig. 2; if viewed from the top down, the data in columns A + B and A − B visualize the build-up and decay profiles commonly found in the exchange spectroscopy.

At this point it also appropriate to discuss the range of applicability of the new experiment. On the slow exchange side, the limitation is imposed by spin relaxation. During the mixing time the magnetization of interest is stored in a form of N_z (Farrow et al. 1994). In unfolded proteins, which are the focus of this study, the longitudinal relaxation of N_z is sufficiently slow, on the order of 1 s^{-1} (in the deuterated sites slower than in the protonated sites). As a result, exchange rates as low as a fraction of 1 s^{-1} can be quantitatively measured. On the fast exchange side, the situation is somewhat more complicated. With an increase in the exchange rate, line broadening leads to deterioration in the signal-to-noise ratio of the spectra and eventually to coalescence of the $^{15}N^H$ and $^{15}N^D$ peaks. Poor INEPT performance compounds the problem (Zangger and Armitage 1998). Furthermore, the exchange mixing prior to τ_{mix} (from point *c* to point *e* in the sequence) and following τ_{mix} (from point *f* to point *g*) can no longer be ignored, which complicates the data analysis. Based on the simulation results, we estimate that the new experiment is suitable for measuring the solvent exchange rates in the range of ~0.2–20 s^{-1}.[2] Note that these estimates are

[2] Our scheme is, therefore, well suited for measurements at or near physiological pH, but cannot be used with acid-denatured samples at pH ~2 where exchange rates are too slow.

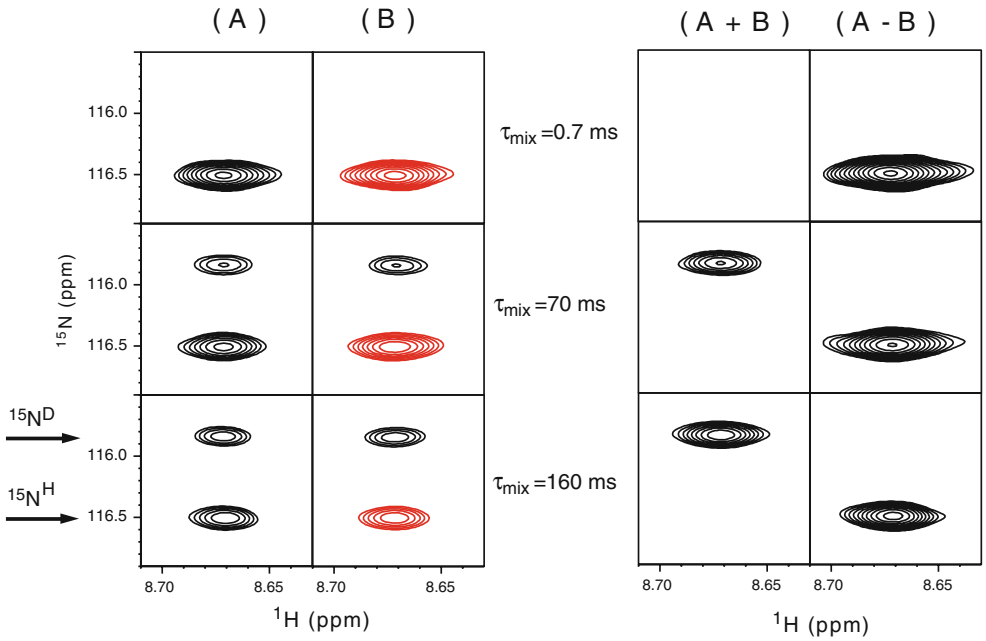

Fig. 2 Regions from $^{15}N^{H/D}$–$^{1}H^{N}$ spectra containing the signals from residue S34 of the chemically denatured drkN SH3 domain. The spectra were recorded using the pulse sequence Fig. 1a for three different values of τ_{mix}, as indicated in the plot. The columns *A* and *B* display the spectra obtained with the initial conditions $+N_x^H, +N_x^D$ and $-N_x^H, +N_x^D$, respectively (positive contour levels are plotted in *black*, negative contour levels in *red*). The results of the addition and subtraction of these spectra are shown in the columns labeled $A + B$ and $A - B$

dependent on the sample concentration, measurement temperature, etc. Experimentally, high-quality data were obtained in the range of 0.3–5 s^{-1} (see below).

Results and discussion

Data interpretation

Integrating peak intensities in the spectra such as illustrated in Fig. 2 (right part) produces a pair of build-up/decay profiles for each resolved signal. The data have been obtained for 35 amides out of 57, with the rest unavailable because of spectral overlaps (same as in the conventional HSQC spectrum of drkN SH3 in 2 M GdnCl). Shown in Fig. 3 are the examples of the build-up/decay curves for the rapidly exchanging residue S34, as well as the slowly exchanging residues I48 and R38 (the latter is a residue of special interest, see below).

A theoretical analysis commonly used in the exchange spectroscopy relies on the following simple evolution equation (McConnell 1958; Jeener et al. 1979):

$$\frac{d}{d\tau}\begin{pmatrix} N_z^H(\tau) \\ N_z^D(\tau) \end{pmatrix} = \begin{pmatrix} -R_1^{NH} - k_{HD} & k_{DH} \\ k_{HD} & -R_1^{ND} - k_{DH} \end{pmatrix} \begin{pmatrix} N_z^H(\tau) \\ N_z^D(\tau) \end{pmatrix} \quad (1)$$

where τ runs from 0 to τ_{mix}. For the pulse sequence at hand, Fig. 1a, the coherence $N_z^H(\tau_{mix})$ is passed for detection, whereas $N_z^D(\tau_{mix})$ is discarded. Assuming that the filtering scheme performs perfectly, the initial conditions should be set to $(N_z^H(0), 0)$ in order to emulate the decay profile and to $(0, N_z^D(0))$ in order to reproduce the build-up profile. With these provisions, Eq. 1 can be readily used to fit the experimental data with k_{DH}, k_{HD}, R_1^{NH}, R_1^{ND}, $N_z^H(0)$, and $N_z^D(0)$ in the role of fitting parameters.

In practice, certain modification can be introduced into the fitting scheme. It has been found that deuteron/proton fractionation factors for backbone amides are similar to 1.1; in particular, this is true for random-coil peptides (Englander and Poulsen 1969; LiWang and Bax 1996). Therefore, the following constraint can be imposed during the fitting: $k_{HD} = 1.1k_{DH}$. As for the ratio of N_z^H and N_z^D magnetizations prior to the beginning of the mixing period, it depends not only on the fractionation factor, but also on the spin relaxation prior to the τ_{mix} period (nitrogen relaxation rates are different for the protonated and deuterated sites). Therefore, we prefer to treat $N_z^H(0)$ and $N_z^D(0)$ as two independent fitting parameters.

In addition, if one assumes that the filtering scheme does not perform perfectly, then the initial conditions $(0, N_z^D(0))$ need to be replaced with $(\varepsilon_H, N_z^D(0))$. In principle, a

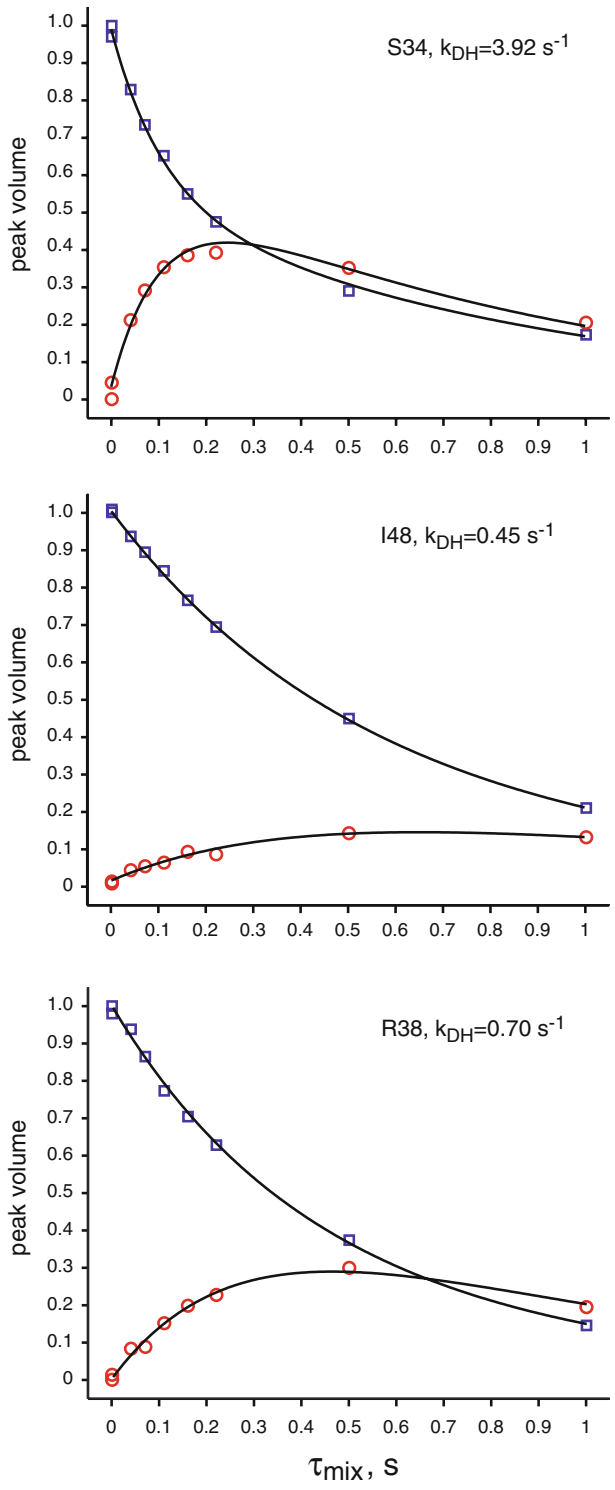

Fig. 3 Build-up/decay profiles for residues S34, I48, and R38. The symbols are: (*square*) volume of the 'axial peaks' (initially protonated amides that remain protonated, cf. Fig. 2, column $(A - B)$), (*circle*) volume of the 'cross-peaks' (initially deuterated amides that become protonated, cf. Fig. 2, column $(A + B)$), (*line*) the results of the fitting using the standard interpretation (see text). In terms of the fitting residual, the shown residues rank 28, 4, and 21 out of 35 investigated sites

symmetric term ε_D should be introduced in the analysis of the decay profile; however, ε_D does not directly contribute to the observable and, therefore, we found it dispensable. In summary, the final set of the fitting parameters is comprised of k_{DH}, R_1^{NH}, R_1^{ND}, $N_z^H(0)$, $N_z^D(0)$, and ε_H.[3]

The results of the fitting procedure using this basic model are illustrated in Fig. 3 for three representative residues, S34, I48, and R38. Similar high-quality fits have been obtained for all other residues in the data set (not shown). The extracted exchange rate constants are summarized in Fig. 4. Note, that our experiment determines the deuterium-to-proton exchange rate k_{DH}, which is encoded in the initial slope of the build-up curve. The initial slope is, in fact, proportional to $k_{DH}N_z^D(0)$; as a consequence, there is a certain amount of 'coupling' between the two parameters. It is this coupling that is primarily responsible for the k_{DH} error bars shown in the plot. The precision would improve if we could observe the signals from the deuterated amide groups, thus getting a handle on $N_z^D(0)$.[4]

As far as relaxation rates are concerned, the extracted values of R_1^{NH} and R_1^{ND} vary from residue to residue. However, the sum of the determined rates $R_1^{NH} + R_1^{ND}$ proves to be nearly constant (mean value 2.5 ± 0.3 s^{-1}) and in good agreement with the theoretical predictions. This behavior is to be expected in a system undergoing relatively fast interconversion between the two states—in such a system only the effective relaxation rate $(R_1^{NH} + R_1^{ND})/2$ can be captured with good accuracy. Finally, the relative amount of $N_z^D(0)$ and $N_z^H(0)$ magnetization was found to be, on average, 1.4 ± 0.3. This is also in line with expectations (see next section for discussion). The 'leakage ratio' of the filter, $\varepsilon_H/N_z^H(0)$, proved to be, on average, 0.02. This latter parameter can be readily visualized as it corresponds to the starting point of the build-up curve, which lies slightly above zero.

Alternative data interpretation

The analysis above raises a few questions. The modestly-sized error bars in Fig. 4, as obtained from Monte Carlo simulations, suggest that the fitting procedure is stable. Nevertheless, it would be helpful to re-fit the data using the independently estimated amplitudes of $N_z^D(0)$ and $N_z^H(0)$. It is also of interest to address the issue of exchange mixing outside τ_{mix}. The problem of poorly defined mixing time is

[3] The convergence of the fitting procedure generally presents no problem; for several residues it is recommendable to first fit the data with $(0, N_z^D(0))$ initial conditions and then use the results as a starting point for the optimization involving $(\varepsilon_H, N_z^D(0))$.

[4] In principle, such an experiment providing a full complement of two 'axial peaks' and two 'cross-peaks' can be designed using a HA(CACO)N-type sequence, although the detection of ^{1}H resonances near the residual water line presents some practical difficulty.

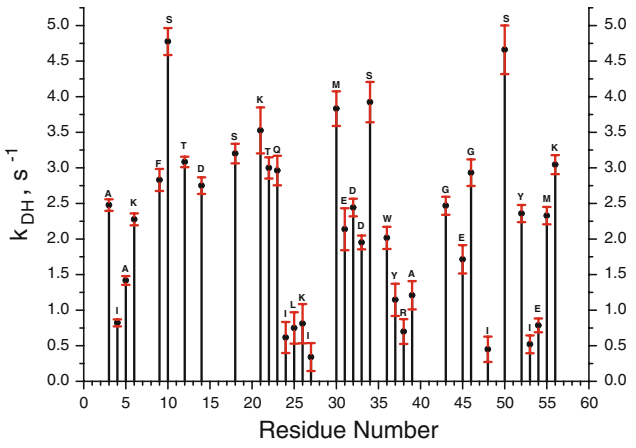

Fig. 4 Exchange rate constants, k_{DH}, as extracted from the standard interpretation of the experimental data. *Error bars* are obtained by analyzing multiple copies of the spectra with added noise (see Sect. "Materials and Methods"). The residue-to-residue variation of the exchange rates is primarily due to the amino acid sequence effects, as discussed later

a general one in exchange spectroscopy (Ernst et al. 1987). In the context of our measurements, it is expected that the exchange mixing during t_1 can be safely neglected. Indeed, an exchange process with a rate of $\sim 1\ s^{-1}$ cannot efficiently couple two coherences precessing at significantly different frequencies, $\omega_{NH} - \omega_{ND} \sim 350\ s^{-1}$ (corresponding to 0.7 ppm isotopic shift). The situation is different in the case of the INEPT elements. There the chemical shift evolution is largely canceled out by refocusing 180° pulse and, as a consequence, exchange mixing becomes possible (Tollinger et al. 2001). To quantify this effect in the context of our semi-constant-time scheme, we have implemented an alternative fitting procedure. In what follows, we describe the simulation protocol employed in this alternative procedure.

In brief, we have simulated the evolution of nitrogen magnetization in the interval between points c and g in the pulse sequence Fig. 1a. The evolution during τ_{mix} was modeled based on Eq. 1, as before; outside the mixing period Eq. 2 was employed:

$$\frac{d}{dt}\begin{pmatrix} N_x^H(t) \\ N_x^D(t) \end{pmatrix} = \begin{pmatrix} -R_{2,eff}^{NH} - k_{HD} - i\omega_{NH} & k_{DH} \\ k_{HD} & -R_{2,eff}^{ND} - k_{DH} - i\omega_{ND} \end{pmatrix} \times \begin{pmatrix} N_x^H(t) \\ N_x^D(t) \end{pmatrix} \quad (2)$$

Eq. 2 provides an empirical description where the effective relaxation rates, $R_{2,eff}^{NH}$ and $R_{2,eff}^{ND}$, represent the losses associated with various in-phase and antiphase coherences evolving between points c and e (also f and g). The decay rates are assumed to be proportional to the experimentally determined nitrogen linewidths, $R_{2,eff}^{NH} + k_{HD} = \pi\delta\nu_{NH}$, $R_{2,eff}^{ND} + k_{DH} = \pi\delta\nu_{ND}$. It is also assumed that the refocusing nitrogen 180_x° pulses reverse the direction of precession, whereas the encoding proton $90_x^\circ 90_{\pm x}^\circ$ pulse alternates the sign of the N_x^H coherence. The initial conditions at point c are set according to the fractionation factor, $N_x^D/N_x^H = 1.1$. The coherence N_x^H evaluated at point g is treated as an observable.

Using this simple theoretical framework, we generated the t_1-domain signal that was sampled with the dwell time of 210 μs to the maximum of 69.7 ms (in analogy with our experimental setup). The simulated signal was subsequently zero-filled, convolved with the window function, and fitted with the Gaussian contour, thus mimicking the actual spectral processing. The line integrals extracted in this manner were compared with the experimental values, and the process was iterated until a good agreement between the experimental and simulated profiles was reached. The resulting fitting procedure employs only four adjustable parameters—k_{DH}, R_1^{NH}, R_1^{ND}, and $N_z^H(0)$—which is two fewer than the protocol discussed in the previous section.

As it turns out, the quality of the fitting remains good throughout the entire data set, with the residual χ increasing only marginally from 0.045 per residue to 0.057 per residue. The extracted k_{DH} rates are in good agreement with the previously obtained values (correlation coefficient $r = 0.94$, *rms* deviation 0.42 s^{-1}, bias less than 0.01 s^{-1}). On the other hand, moderate differences are observed for several residues that show an appreciable amount of noise. For instance, the biggest difference is found in K21: $k_{DH} = 3.5\ s^{-1}$ in the conventional analysis versus 2.3 s^{-1} in the alternative interpretation. Incidentally, K21 is a weak peak with an unusual amount of line broadening that gives rise to the largest fitting residual χ in both conventional and alternative analyses (0.085 and 0.130, respectively).

As far as the other parameters are concerned, the average ratio of $N_z^D(0)$ and $N_z^H(0)$ prior to the beginning of the mixing period was found to be 1.4 ± 0.4, and an average 'leakage ratio' of the filter turned out to be 0.02. Both values are the same as obtained previously. This is a satisfying result because in the conventional interpretation these quantities are treated as fitting parameters, whereas in the alternative interpretation they are modeled on the basis of the experimental nitrogen linewidths.

Generally, the alternative interpretation should not be regarded as more accurate. Indeed, the description involving Eq. 2 is fairly crude. It is, however, more physically sound and less prone to overfitting. The agreement between the two treatments is, therefore, reassuring—the more solid (yet technically cumbersome) alternative analysis lends support to the conventional scheme. In what follows, we focus on the k_{DH} rates extracted by means of the conventional treatment, Fig. 4.

Comparison with CLEANEX-PM experiment

The CLEANEX-PM sequence (Hwang et al. 1997; Hwang et al. 1998) is a result of a long line of development of saturation-transfer experiments. In the beginning of the sequence, a (gradient)–(selective pulse)–(gradient) combination is used to destroy $^1H^N$ magnetization, while at the same time preserving H_2O magnetization. During the subsequent mixing period the protons are effectively locked at the angle of 35° to the static magnetic field; this particular setting of the lock angle ensures that the Overhauser transfer is canceled in large molecules (i.e., in those molecules where the motional correlation time exceeds several nanoseconds; Griesinger and Ernst 1987; Cavanagh and Rance 1992; Desvaux et al. 1995). Likewise, the TOCSY transfer is inefficient under these conditions. With the unwanted pathways blocked, CLEANEX-PM monitors the flow of magnetization from water to amides due to the solvent exchange.

As already pointed out in the introduction, the CLEANEX experiment is potentially affected by a number of issues—some of them of general character, others related to unfolded proteins. First, water manipulations present a host of potential problems. Application of the weak gradient during the mixing time—seeking to prevent radiation damping and, at the same time, retain the spin lock conditions—has never been critically probed. Special care is required to determine the degree of water saturation due to the short recycling delays and the loss of magnetization during the selective pulse (see Sect. "Materials and Methods"). Note that the measurements involving water signal can become especially problematic in a situation when the rf heating (see below) causes thermal convection in a sample. A hidden bias at this stage can lead to a systematic error in the determined exchange rates.

Secondly, there are conceptual difficulties. For unfolded proteins spin relaxation is strongly influenced by sub-nanosecond motions (Farrow et al. 1995, 1997). As a result, the cancelation of the Overhauser effect may become less than perfect, as pointed out already by the authors of CLEANEX (Hwang et al. 1998). Although NOESY cross-peaks in unfolded proteins are positive and the compensation scheme using 35° tilt angle should remain reasonably efficient (Schleucher and Wijmenga 2002), one cannot rule out the presence of a small amount of the NOE-mediated transfer. In particular, this unwanted mechanism may facilitate $^1H^\alpha$-to-$^1H^N$ transfer (some of $^1H^\alpha$ protons resonate close to the water line and, as a consequence, may retain their magnetization and then feed it to the amide protons). Finally, one cannot fully discount the presence of the water-to-protein intermolecular NOE transfer. While the effect is expected to be small, less than 0.1 s^{-1} (Otting et al. 1991; Modig et al. 2004), it is not compensated for by the CLEANEX sequence. In the end, one cannot exclude the possibility that several minor contributions may combine and introduce an appreciable error in the outcome of the experiment.

Thirdly, there are certain technical difficulties encountered in samples with high ionic strength, and specifically those using the common guanidinium chloride (GdnCl) denaturant. The powerful proton spin lock applied during the CLEANEX mixing period causes significant amount of heating in such samples. For example, the temperature rises by 4.3°C in our measurement on drkN SH3 in 2 M solution of GdnCl using a long mixing time, 150 ms (see Sect. "Materials and Methods"). This amount of heating causes a dramatic 50% speed-up in the solvent exchange rates (Bai et al. 1993), which clearly compromises the results of the experiment. It further causes noticeable drift of the amide resonances, which makes it impossible to rely on the autofit procedure to quantify the peak intensities—a significant setback in the case of weaker peaks (see Sect. "Materials and Methods").

With all these actual and potential complications in mind, we decided to compare the results from CLEANEX-PM and the new experiment described in this work. As discussed above, our experiment uses the ^{15}N spin instead of ^1H to target solvent exchange. As a result, it is free of the problems described above. A good agreement between the two experiments would provide a strong endorsement for future use of CLEANEX in applications involving unfolded (disordered) proteins. At the same time, it would validate our hitherto untested scheme.

The CLEANEX experiment was set up as described in the "Materials and Methods" section and interpreted according to Eq. 1 in the original publication (Hwang et al. 1998). The fitting protocol involves two adjustable parameters: the exchange rate $k = p_H k_{HH} + p_D k_{DH}$ (where p_H and p_D denote the fraction of protonated and deuterated amide sites, respectively) and the effective relaxation rate $R_{1\rho}^H$ for amide proton magnetization locked off-resonance. In the linear region of the build-up curve (initial slope regime), only k is fitted in a meaningful fashion. Considering the slight preference of amide sites for deuterium, $p_D/p_H = k_{HD}/k_{DH} = 1.1$, and focusing on the sample at hand, 50% H_2O–50% D_2O, it is easy to estimate that $k = 1.025\, k_{DH}$. This 2.5% correction has been applied to the CLEANEX rates prior to comparing the results from the two measurements.

The CLEANEX fits using all available data points have been clearly problematic, showing substantial systematic deviations at $\tau_{mix} = 150$ ms (not shown). Given the amount of heating that occurs at the long mixing times, this is not surprising. To avoid these complications, we restricted the data set to $\tau_{mix} \leq 50$ ms (typical choice for CLEANEX

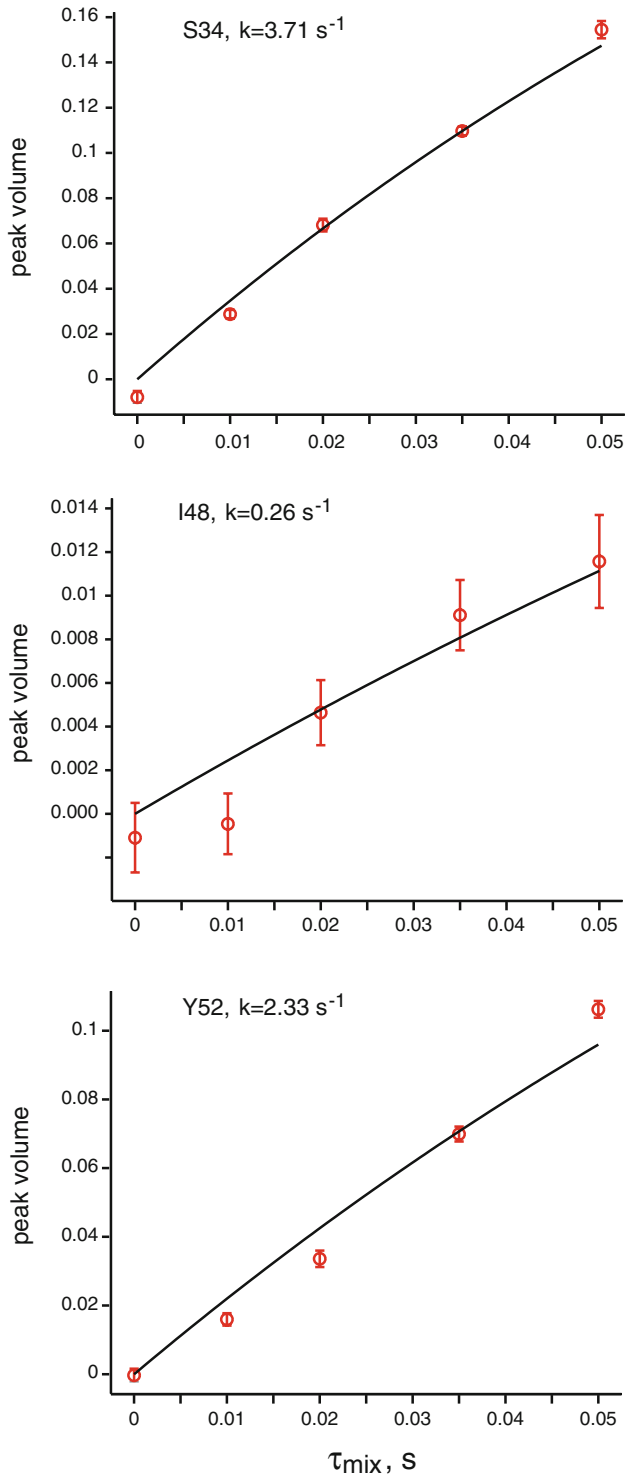

Fig. 5 CLEANEX-PM build-up profiles for residues S34, I48, and Y52. *Error bars* are obtained from multiple copies of the spectra with added noise

experiment) and re-analyzed the data. The representative examples are shown in Fig. 5.

Residue S34 shows a fairly typical good-quality fit, with just a hint of a possible systematic problem. It is a rapidly exchanging residue, giving rise to strong CLEANEX peaks; the extracted rate, $k = 3.7\ s^{-1}$, is consistent with the one measured using the new pulse sequence, $k_{DH} = 3.9 \pm 0.3\ s^{-1}$. The residue I48, on the other hand, gives an example of poor performance. This residue is a slow exchanger—as a result, very little magnetization is transferred over the period of 50 ms, resulting in an obvious sensitivity issue. While the rates from the two experiments nearly agree within the error margin, $k = 0.26\ s^{-1}$ versus $k_{DH} = 0.45 \pm 0.18\ s^{-1}$, this example demonstrates how CLEANEX measurements are limited by the length of the mixing time.[5] The main concern with the CLEANEX experiment, however, is not the sensitivity limit affecting slowly exchanging residues, but rather the potential presence of systematic errors. One of a number of residues showing signs of systematic problems is Y52 (bottom panel in Fig. 5). It is difficult to speculate on the origin of the observed discrepancies; we merely notice that the extracted rate remains consistent with our previous results, $k = 2.3\ s^{-1}$ versus $k_{DH} = 2.4 \pm 0.1\ s^{-1}$.

Finally, we summarize the exchange rate data in Fig. 6. The correlation between the results from CLEANEX and $^{15}N^{H/D}$-SOLEXSY is good beyond expectations: the correlation coefficient is $r = 0.97$, the rms deviation $0.30\ s^{-1}$, bias less than $0.1\ s^{-1}$. Both experiments apparently perform reasonably well and, in the case of CLEANEX, potential complicating factors do not seem to cause any major errors, at least for this particular chemically denatured protein sample.

Protection factors

To interpret the experimentally measured exchange rates, it is necessary to relate them to the so-called random-coil rates, k_{rc}. The ratio of these two quantities defines the protection factor (PF), which is taken to describe the slowdown in solvent exchange due to the presence of the (native-like or non-native) structure. The k_{rc} rates can be extrapolated from data collected by Englander and co-workers (Bai et al. 1993; Connelly et al. 1993). In our case, the standard protocol needs to be slightly modified to specifically address deuterium-to-proton exchange in 50% H_2O–50% D_2O solvent. Details of k_{rc} calculations are summarized in the "Materials and Methods" section.

Values of the protection factors, based on data from the $^{15}N^{H/D}$-SOLEXSY experiment, are shown in Fig. 7. For most residues, the values fall between 0.5 and 2. Variations within this range cannot be considered meaningful since they are mostly caused by the uncertainty in the calculated

[5] There is another slowly exchanging residue, I27, which yields an exchange rate $0.34 \pm 0.20\ s^{-1}$ in our experiment, but cannot be detected in the CLEANEX spectra.

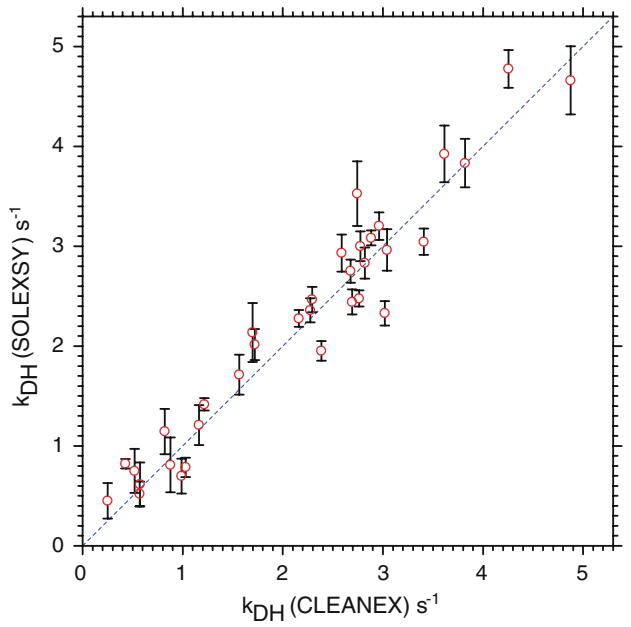

Fig. 6 Solvent exchange rates from the $^{15}N^{H/D}$-SOLEXSY experiment (k_{DH}) and CLEANEX-PM experiment ($k_{DH} = k/1.025$)

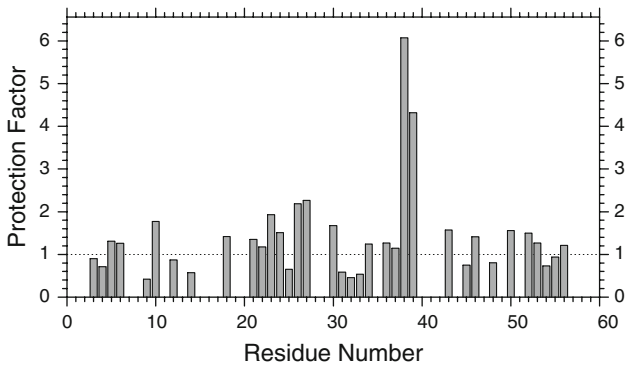

Fig. 7 Protection factors in the 2 M GdnCl denatured state of drkN SH3 obtained from the $^{15}N^{H/D}$-SOLEXSY measurements interpreted using the standard protocol (see text). The highest PF value, 6.1, is observed in residue R38 (build-up and decay profiles for this residue are shown in Fig. 3)

k_{rc} values (Buck et al. 1994; Koide et al. 1995; Mori et al. 1997). For instance, Glu and Asp residues show systematically low protection factors—0.59, 0.75, 0.73 and 0.57, 0.46, 0.53 for three observed residues of each type. Gly residues, on the other hand, show higher-than-expected protection factors, 1.57 and 1.41. These results are quantitatively similar to what has been reported by Mori et al. for staphylococcal nuclease Δ131Δ in water, although somewhat different from the values found in 2 M GdnCl (on average, 0.30 for Glu and Asp and 1.23 for Gly; Mori et al. 1997). In principle, careful measurements of exchange rates in several unfolded proteins with random-coil-like behavior (Wirmer et al. 2006) can be used to re-calibrate the reference k_{rc} rates.

The salient feature of the plot Fig. 7 is the high protection factors of the two contiguous residues, R38 and A39. Remarkably, they appear at the same spot where elevated protection factors were previously observed in the sample of the unfolded state of drkN SH3 under non-denaturing conditions (Crowhurst et al. 2002). This result is surprising. High protection factors in the unfolded drkN SH3 were previously interpreted as the evidence of hydrophobic burial. Now this interpretation needs to be re-examined since it is unlikely that any significant hydrophobic cluster would be present in the 2 M GdnCl denatured state of drkN SH3 (Kohn et al. 2004).

Origin of high protection factors in drkN SH3

The small marginally stable drkN SH3 domain has been a subject of extensive studies seeking to establish a structural model for disordered proteins (Marsh and Forman-Kay 2009). When dissolved in aqueous buffer at or near neutral pH, drkN SH3 exists in dynamic equilibrium between the folded state (populated to about 60%, termed F_{exch}) and the unfolded state (40%, U_{exch}). The F_{exch} form is a typical globular domain with the standard β-barrel fold found in other SH3 domains (Bezsonova et al. 2005). The U_{exch} form, which received most attention, is a disordered protein that has been described as relatively compact with some non-random structural features, including fluxional hydrophobic cluster centered at residue W36.

As a point of reference, the chemically denatured state of drkN SH3 has also been investigated (U_{Gdn}, 2 M GdnCl, same as studied in this work). It has been demonstrated that U_{Gdn} has a substantially larger radius of gyration than U_{exch} (Choy et al. 2002; Marsh and Forman-Kay 2009). The radius of gyration for U_{Gdn} is in line with other strongly denatured proteins (Kohn et al. 2004), suggestive of random-coil behavior. At the same time, various NMR data indicate that the behavior of U_{Gdn} is more complex than would be expected of an ideal random coil (Farrow et al. 1997; Crowhurst and Forman-Kay 2003; Xue et al. 2009).

In Table 1 we summarize the protection factors reported previously by Crowhurst et al. for the U_{exch} state (Crowhurst et al. 2002) and obtained by us for the U_{Gdn} state. The results in the first two columns suggest that the apparent protection pattern in U_{exch} and U_{Gdn} is similar. Of particular interest are the sites displaying a high degree of protection (indicated in bold). One possible explanation for PF values $\sim$5, such as found in residues R38 and A39, would be to suggest that these particular residues are locked in hydrogen bonds for 80% of the time, while being fully exposed to solvent for the remaining 20% of the time. This scenario, however, is rather improbable given that both states, U_{exch} and U_{Gdn}, are highly dynamic. Otherwise, elevated protection factors may arise as a result of

Table 1 Protection factors for residues surrounding W36 in the U_{exch} state (Crowhurst et al. 2002) and U_{Gdn} state (this work) of the drkN SH3 domain

Residue	U_{exch}	U_{Gdn}	
	Protection factors (k_{rc} calculated)	Protection factors (k_{rc} calculated)	Protection factors (k_{rc} experimental)
N35	**2.9**	–	–
W36	1.9	1.3	•
W36 indole	est. **>10**	2–**4**	0.8
Y37	2.1	1.1	•
R38	**5.6**	**6.1**	•
A39	–	**4.3**	0.9

The backbone data in the middle column are the same as plotted in Fig. 7; the data from the W36 side-chain indole are described separately in the text. For certain residues the data are unavailable because of spectral overlaps (indicated by a dash) or the absence of reference peptide samples (indicated by a dot). The values suggesting a significant degree of protection (presumed to be outside the uncertainty range associated with k_{rc}) are indicated in bold

hydrophobic burial of certain central residues. While this hypothesis cannot be a priori ruled out for the U_{exch} state, it is unlikely to be valid for U_{Gdn} which is highly expanded. Hence, we turn to an alternative explanation, assuming that the apparent increase in protection factors is an artefact arising from the calculation of k_{rc}.

As already pointed out, the calculations of k_{rc} can be a source of sizeable uncertainty (Buck et al. 1994; Koide et al. 1995; Mori et al. 1997). While the model used for calculations has been carefully calibrated (Bai et al. 1993; Connelly et al. 1993), it involves a number of simplifying assumptions. It also relies on extrapolation to reproduce various experimental conditions such as temperature, ionic strength of the solution, etc. A simple workaround is to synthesize a short peptide with the sequence derived from that of the drkN SH3 domain and measure the exchange rates in this peptide under the same conditions as used in the protein experiments.

In pursuing this approach, we prepared a sample of a WYRAEL peptide which corresponds to a fragment from the drkN SH3 sequence. The peptide has been labeled with ^{15}N in the alanine position equivalent to A39; the solvent and other experimental conditions were the same as in the protein experiments. The exchange rate of the alanine amide was measured using the CLEANEX-PM sequence and found to be $k_{DH}^{pept}(=k_{rc}) = 1.09\ s^{-1}$. This is to be compared with 1.21 s^{-1} obtained for residue A39 in the sample of denatured drkN SH3 using the $^{15}N^{H/D}$-SOLEXSY experiment (or 1.16 s^{-1} using CLEANEX). The protection factor, therefore, comes equal to 0.9, which is distinctly different from the previously obtained value 4.3.

Of special interest is the W36 side-chain indole site, where a high degree of protection has been assumed by Crowhurst et al. (see Table 1). Previous CLEANEX measurements on the F_{exch}/U_{exch} sample detected no exchange peaks for this site, leading to the estimated $k < 0.3\ s^{-1}$. Given that the intrinsic exchange rate of the tryptophan $H^{\varepsilon 1}$ under the given experimental conditions is ca. 3 s^{-1}, it has been estimated that PF > 10 (Crowhurst et al. 2002). Similar to Crowhurst et al., we also failed to observe an exchange peak from the indole $H^{\varepsilon 1}$ in the CLEANEX experiment (a very weak peak actually appears in the spectrum recorded with exceedingly long mixing time, $\tau_{mix} = 150$ ms). As it later became clear, the poor performance of CLEANEX is due to the slow exchange of $H^{\varepsilon 1}$ proton; it is also likely that the CLEANEX spin lock does not perform well for the indole resonance located far downfield in the spectrum.

In this situation, we resorted to the e-PHOGSY scheme (Dalvit and Hommel 1995; Dalvit 1996), which allows for much longer mixing times.[6] The measurements were successful, leading to $k_{DH} = 0.39\ s^{-1}$ in the U_{Gdn} state. To calculate the reference rate, k_{rc}, we relied on the data from a model dipeptide, N-acetyl tryptophan N′-methyl amide (Bai et al. 1993). Using these data, the k_{rc} rate is predicted to be 0.7–1.5 s^{-1} (depending on whether the denaturant correction (Loftus et al. 1986) is applied or not). Hence, the protection factor is estimated to fall in the range PF = 2 − 4 (see Table 1). A similar result is obtained if L-tryptophan (Skrynnikov and Ernst 1999) is used as a reference compound.

Given the approximate nature of the above prediction, it is desirable to directly determine the reference rate. For this purpose, we have investigated the GGWGG and SNWYR peptides, of which the latter derives from the drkN SH3 sequence. Using the homonuclear version of the e-PHOGSY experiment, we have measured the respective indole exchange rates, $k_{DH}^{pept} = 0.38\ s^{-1}$ and 0.33 s^{-1}. Taking the second value to represent k_{rc}, we arrive at the protection factor 0.8 for the W36 indole in the denatured form of the protein, U_{Gdn} (Table 1).[7]

[6] It can be pointed out that the e-PHOGSY scheme does not protect against the Overhauser transfer. This, however, is also true for CLEANEX outside the macromolecular limit. Given our successful validation of CLEANEX in this work, this does not appear to be a significant problem.

[7] In addition, we have determined the protection factor for the W36 indole in the salt-stabilized F_{exch} state, PF = 1.9. This result is in line with expectations since the tryptophan side chain is fully exposed to solvent in the folded protein. It is also consistent with the previous observations that W36 has the same (high) degree of solvent exposure in the F_{exch} and U_{exch} states (Evanics et al. 2006 Biochemistry 45:14120–1412). Note that in this study the exchange of W36 $H^{\varepsilon 1}$ proton with solvent, as quantified by e-PHOGSY, was mistakenly described as water NOE.

The results obtained with reference peptides suggest that the elevated protection factors in the U_{Gdn} state (and, by extension, in U_{exch}) are most likely artefacts arising from calculation of k_{rc}. In retrospect, this is not so surprising—while most of the protection factors reported in the literature fall in the range 0.5–2, values on the order of 0.2–0.3 have also been observed (Mori et al. 1997; Crowhurst et al. 2002). Therefore, one can as well expect to encounter values of 3–5, which merely reflect uncertainty in the k_{rc}. One may ask if there is any reason why the calculated k_{rc} values turn out to be significantly overestimated in the two consecutive residues, R38 and A39. Currently, we do not know the answer to this question. Some of the hypothetical scenarios can be ruled out. For instance, one can speculate that phosphate ions (contained in the buffer solution) may weakly interact with this particular site, causing a slow-down in solvent exchange. Similar examples have been described in the literature (Delepierre et al. 1987). This is, however, not the case for U_{Gdn} as we were able to reproduce our results in a Tris buffer (data not shown).

Finally, let us discuss the significance of our observations in relation to the general view of the U_{exch} state. The latest studies describe U_{exch} as a large and heterogeneous ensemble of conformations, where multiple hydrophobic groups make transient contacts with each other (Marsh and Forman-Kay 2009). While the pattern of hydrophobic contacts is diverse—some are native-like, others non-native—it clearly differentiates the U_{exch} state from a featureless random coil. However, careful review of the experimental data, including the amide exchange data presented in this work, suggests that these transient contacts do not produce the effect of hydrophobic burial. Further research into the nature of U_{exch} state using the ENSEMBLE approach (Choy and Forman-Kay 2001; Marsh and Forman-Kay 2009) is currently underway.

Concluding remarks

Among many experimental techniques used in studies of disordered proteins, NMR spectroscopy plays a leading role. The acquired data, however, tend to be less informative than in the case of folded proteins. In the situation where structural data are scant, hydrogen exchange can be a valuable source of information. The exchange data are usually expressed in a form of protection factors, i.e., in relation to ideal random-coil values. In the case of molten globules, protection factors vary in a relatively wide range, ~1–1000 (Schulman et al. 1995; Nishimura et al. 2008). In highly disordered proteins the range is smaller, ~1–10. Nevertheless, such data have been used to identify nascent helices (Yao et al. 2001), hydrophobic clusters (Crowhurst et al. 2002), structural features associated with disulphide bridges (Forge et al. 1999), etc.

In the context of exchange measurements in disordered proteins there are two lessons that can be learned from the present study. First, it is not a priori clear that the proton-based exchange experiments developed for folded proteins can be safely applied to the unfolded proteins. For example, the Overhauser effect compensation scheme implemented in the CLEANEX-PM experiment is not necessarily expected to work for flexible peptide chains. It is, therefore, desirable to validate the existing measurement schemes. Such validation is provided by the nitrogen-based $^{15}N^{H/D}$-SOLEXSY experiment described in this paper. The new method uses nitrogen spin as a probe of solvent exchange, thus avoiding numerous complications associated with protons.

Second, our results call for caution in interpreting the protection factors of disordered proteins. The obvious bottleneck in determination of protection factors is the limited accuracy of the calculated random-coil rates k_{rc}. Although the prediction algorithm developed by Bai and Englander performs surprisingly well, there is clearly a limit to how accurate the predicted values can be (Buck et al. 1994). While in most cases the accuracy is sufficient to localize the PFs in the interval from 0.5 to 2, the values as high as 5 and even 10 can apparently occur as a result of uncertainty in k_{rc}. Every time that such elevated PF values are encountered, it would be wise to verify the result by investigating an appropriate peptide model. The k_{rc} rate directly measured in a five- or six-residue peptide under the experimental conditions identical to that of the protein experiment should provide a reliable reference. Only those PF values that have been validated in this manner can be safely used as markers of non-random structure.

In principle, one may envisage that the experimental k_{rc} values can be obtained for an entire library of peptides representing a small protein such as drkN SH3. In conjunction with an accurate measurement technique, this could greatly improve the quality of the PF data and make them sensitive to even a small content of non-random structure. Such improved data can be then incorporated into computational protocols to model the complex behavior of disordered proteins (Delepierre et al. 1987; Vendruscolo et al. 2003; Best and Vendruscolo 2006; Marsh and Forman-Kay 2009).

Finally, the new experimental approach can be particularly useful for studies of amide solvent exchange in solid-state NMR (Harbison et al. 1988; Lesage and Böckmann 2003; Chevelkov et al. 2005; Lesage et al. 2008). Handling of proton magnetization in solids is especially difficult, greatly exacerbating the problems encountered in saturation-transfer experiments. As an alternative strategy, indirect detection of solvent exchange via ^{15}N spin probe offers

significant benefits. Toward this goal, the described EXSY scheme can be adapted for use with deuterated samples employing ^{13}C detection. Knowledge of effective pH and amide exchange rates in hydrated protein crystals is important for studies of internal protein dynamics by means of the solid-state NMR (Chevelkov et al. 2007).

Materials and methods

Samples

To validate the new experimental scheme we prepared a uniformly ^{13}C,^{15}N-labeled sample of the 59-residue N-terminal SH3 domain of the *Drosophila* adapter protein drk (drkN SH3; Zhang et al. 1994). The sample conditions were 1 mM protein, 50% H_2O–50% D_2O solvent, 2 M guanidinium chloride (GdnCl), 50 mM sodium phosphate. Chemical shift titration and chevron plot data suggest that the protein is almost fully denatured in the presence of 2 M GdnCl (Mok et al. 2001; Crowhurst et al. 2002). All measurements were conducted at 5°C, where the conditions for observation were found to be optimal. The pH was carefully measured at the working temperature 5°C; to account for glass electrode isotope effect in the 50% H_2O–50% D_2O solvent the reading of the meter (pH 7.5) was corrected by 0.2 units (pH 7.7). The spectral assignment were obtained from the previous report (Zhang and Forman-Kay 1997) and confirmed by a CBCANH experiment (Grzesiek and Bax 1992).

Additional measurements were performed on (1) a 1 mM sample of ^{15}N-labeled drkN SH3 in 2 M GdnCl with 50 mM Tris instead of 50 mM phosphate, (2) 1 mM sample of ^{15}N-labeled drkN SH3 in the folding buffer (500 mM sodium sulphate, 50 mM sodium phosphate), and (3) 2 mM samples of GGWGG and SNWYR peptides (unlabeled, obtained from Peptide 2.0 Inc., Chantilly, VA), as well as WYRAEL peptide (labeled with ^{15}N in the alanine position, obtained from Biopeptide Co. Inc., San Diego, CA) in 2 M GdnCl, 50 mM phosphate buffer. All buffers were prepared using 50% H_2O–50% D_2O solvent, with uncorrected pH adjusted to 7.5.

NMR experiments

In the pulse sequence Fig. 1a narrow and wide shapes indicate 90° and 180° pulses, respectively. The duration of the ^1H hard 90° pulse is 22 μs (about two times longer than usual because of the high ionic strength of the 2 M GdnCl solution). Proton decoupling is accomplished using a DIPSI-2 sequence (Shaka et al. 1988) with rf power of 1.5 kHz. The WATERGATE water-suppression scheme makes use of the 3-9-19 pulse train (Sklenár et al. 1993). The proton rf carrier is set at the water line (5.2 ppm in the studied sample).

^{13}C rf carrier is initially set at 54 ppm and then jumped to 174 ppm at point *b* in the pulse sequence. The duration of the carbon hard 90° pulse is 10.2 μs (unaffected by the solution ionic strength). Carbon selective pulses are shown in Fig. 1a with rounded shapes. Filled broad shapes represent 180° Q3 pulses (Emsley and Bodenhausen 1992) with 256 μs duration and 13.3 kHz maximum power. Open broad shape represents 180° Q3 pulse with 1 ms duration and 3.4 kHz maximum power (selective with respect to $^{13}C^{\alpha}$ vs. $^{13}C^{\beta}$). Hatched shapes represent the broadband 180° chirp pulses (Böhlen et al. 1989) with the excitation contour centered at 114 ppm, duration 250 μs, and maximum power 11.2 kHz. Pulses marked with asterisk (*) serve to compensate for the Bloch-Siegert shift (Vuister and Bax 1992); those marked with dagger (†) are 'placeholder' pulses used as a part of the scheme to compensate for ^{15}N chemical shift evolution at $t_1 = 0$. The filled narrow shape represents a 90° G4 pulse (Emsley and Bodenhausen 1990) with 400 μs duration and 12.0 kHz maximum rf power. The open narrow shape is the same, except the pulse uses a time-reversed G4 profile.

The ^{15}N rf carrier is set at 119 ppm; the duration of the nitrogen hard 90° pulse is 38.5 μs. Nitrogen decoupling during the detection period uses a GARP sequence (Shaka et al. 1985) with rf power of 1.39 kHz. The ^2H rf carrier is set at 5.2 ppm. Deuterium decoupling is performed using a WALTZ-16 scheme (Shaka et al. 1983) with 1.25 kHz rf power.

All rf pulses have been applied with the phase *x* unless otherwise indicated. The phase cycle employed is $\phi_1 = 2x, 2(-x)$, $\phi_2 = 4x, 4(-x)$, $\phi_3 = 8x, 8(-x)$, $\phi_4 = x, -x$, $\phi_{rec} = (x, -x, -x, x), 2(-x, x, x, -x), (x, -x, -x, x)$. The durations and strengths of the gradients are (G1) 0.7 ms, 30 G/cm, (G2, G4, G5) 1 ms, 35 G/cm, (G3) 0.5 ms, 35 G/cm. The following optimized INEPT delays have been employed: $\tau_a = 1.5$ ms, $\tau_b = 1.785$ ms, $\tau_c = 4.55$ ms, $\tau_d = 14.16$ ms, $\tau_e = 2.64$ ms, $\tau_f = 2.2$ ms. The recycling delay has been set to 1.3 s.

Phase-sensitive detection in the indirect dimension is accomplished using the TPPI scheme (Marion and Wüthrich 1983) applied to the phase ϕ_4. The semi-constant-time acquisition period has been set up using $\kappa = 0.235$; the time $(1 + \kappa)t_1$ is incremented with the step of 210 μs to the maximum of 69.7 ms. The duration of the t_2 acquisition time is 70 ms. The data corresponding to the initial conditions $+N_x^H, +N_x^D$ and $-N_x^H, +N_x^D$ are recorded in an interleaved fashion and stored in a form of a pseudo-3D

spectrum consisting of the two respective HSQC-type spectral planes (cf. planes (A) and (B) in Fig. 2).[8]

All spectra have been recorded on an 800 MHz Bruker Avance III spectrometer using room-temperature triple-resonance probe. The series of measurements employing the mixing times of 0.7 ms (accommodates the gradient G3; data recorded in duplicate to verify the stability of the experiment), 40.7, 70.7, 110.7, 160.7, 220.7, 500.7, and 1000.7 ms has been completed in 45 h.

The CLEANEX-PM pulse sequence (Hwang et al. 1998) has been downloaded from the standard Bruker pulse sequence library and used without any modifications. The durations and the power of the hard rf pulses were the same as described above. During the mixing time the proton spin-lock field is applied with the power 6.8 kHz and the weak pulsed field gradient is applied with the strength 0.1 G/cm. The series of measurements using nine mixing times –0, 10, 20, 35, 50, 75, and 150 ms (the latter two recorded in duplicate)—takes 24 h to record.

The apparent decay rate constant for the locked water signal is measured in a separate experiment as suggested by (Hwang et al. 1998). Of note, the recorded decay curves are biexponential: the initial ca. 10% drop, which is caused by fast exchange between water and (saturated) guanidinium protons, is followed by steady relaxation decay. It is the latter component that is representative of solvent relaxation. To record a reference spectrum, the CLEANEX sequence was reduced to the basic HSQC and the spectrum was acquired using the same experimental settings as in the original experiment, but with a long recycling delay, 10 s. An additional 1D experiment was implemented to find the degree of saturation of water magnetization. In this experiment, we cycle through the original CLEANEX sequence for 32 scans to bring the system to a steady state. This is followed by the recycling delay and the CLEANEX water-selection element, 90° – gradient – 180°_{sel} – gradient, after which the water signal is recorded. The experiment is repeated with different phase settings on the 180°_{sel} pulse, emulating the phase cycle of the actual CLEANEX sequence. The resulting partially saturated H_2O signal is then compared to the maximum water signal (obtained from a single-pulse experiment with 20 s recycling delay). As it turns out, the state of water depends on the length of the mixing time in the sequence (e.g., for $\tau_{mix} = 0$ the attenuation factor is 0.59, whereas for $\tau_{mix} = 50$ ms it is 0.47). The corresponding corrections have been applied to the CLEANEX data on a point-by-point basis. On this subject, it should be noted that accurate measurements using the CLEANEX sequence require three specialized reference experiments. If these reference experiments are not set up properly, the ensuing error in k can be on the order of tens of percent.

The application of a high-power proton spin lock over an extended period of time in the CLEANEX-PM experiment causes substantial amount of heating, which becomes especially pronounced for the sample at hand because of the high ionic strength of the solution. To quantify this effect, we have relied on the temperature-dependent chemical shifts of amide protons (Baxter and Williamson 1997). To calibrate the dependence of $^1H^N$ shifts on temperature, four conventional ^{15}N–$^1H^N$ HSQC spectra have been recorded at the temperatures ranging from 0 to 15°C. Using this calibration, the amount of heating in the CLEANEX-PM measurements is determined to be 1.3°C for the experiment with $\tau_{mix} = 50$ ms and 4.3°C for $\tau_{mix} = 150$ ms.[9] In contrast, the temperature changes registered in the experiment Fig. 1a are minimal (within 0.1°C).

To measure the alanine exchange rate in the ^{15}N-labeled WYRAEL peptide, we used a 1D version of the CLEANEX PM (Hwang et al. 1997). For measurements involving the slowly exchanging indole site, the CLEANEX sequence was converted into a longitudinal e-PHOGSY (Dalvit and Hommel 1995; Dalvit 1996). In brief, the off-resonance proton spin lock was replaced with a NOE-style mixing period, $90^\circ - \tau_{mix} - 90^\circ$. For the isotopically labeled protein samples, we used a ^{15}N-filtered 1D version of the PHOGSY, whereas for the unlabeled GGWGG and SNWYR peptides the homonuclear version was employed. All reference experiments (see above) have been adapted accordingly.

Spectra processing

The spectrum, originally recorded in a pseudo-3D fashion, was separated into two planes which were subsequently added/subtracted (see Fig. 2). The data were zero-filled to 8096 × 2048 matrix, apodized in both dimensions with 60°-shifted squared sine bell window function, and Fourier-transformed. The processed data represent two 'stacks' of spectral planes, where each plane corresponds to a different τ_{mix} value. The spectra were integrated using the autoFit/nlinLS routines from the NMRPipe package (Delaglio et al. 1995). These routines operate on the entire

[8] In applications involving unfolded proteins, the $^1H^N$,^{15}N spectral map generally offers better resolution than other 2D spectra. However, even in the case of small proteins, such as drkN SH3, there is a significant number of peak overlaps. In principle, this problem can be overcome with the help of reduced dimensionality schemes utilizing $^{13}C'$ and $^{13}C^\alpha$ chemical shifts (Brutscher et al. (1994) J. Magn. Reson. Ser. B 105:77–82; Tugarinov et al. (2004) J. Biomol. NMR 30:347–352).

[9] Note that, in principle, heating effects can be compensated for (Wang and Bax 1993 J. Biomol. NMR 3:715–720).

'stack' of spectral planes, making an assumption that the peak position and the linewidths do not change significantly from one plane to the other and hence can be optimized in a global sense. This approach is especially helpful for quantitation of the weak peaks corresponding to the initial points in the build-up curve. The data were fitted assuming Gaussian peak shapes, as appropriate for the squared sine bell apodization.

To generate the error bars associated with k_{DH} and other fitting parameters (see Fig. 4) we adopted the following approach (Eichmüller and Skrynnikov 2005). The right half of each spectral plane—containing nothing but spectral noise—was extracted, subjected to a cyclical shift in the ^{15}N dimension, and then added to the informative left half of the spectrum. The generated data set was analyzed in exactly the same fashion as the original data set. This manipulation has been repeated 20 times with different realizations of noise (obtained by consecutive application of the cyclical shift to the right half of the spectrum), resulting in a series of twenty fitted k_{DH} values. The standard deviation of this series is used as an error estimate for k_{DH}; the error bars shown in Fig. 4 correspond to the interval $\pm\sigma$.

The ^{15}N linewidths have been evaluated using the analogous procedure, including the autoFit treatment, except that the spectra were processed without the apodization functions and then fitted assuming the Lorentzian peak shape. The treatment of the 2D CLEANEX data was exactly as described above. The 1D CLEANEX and PHOGSY spectra were integrated using Topspin 2.1 (Bruker BioSpin GmbH, Rheinstetten, Germany).

Calculation of reference exchange rates

The 'random-coil' exchange rates for a protein with a given primary sequence under given experimental conditions (pH, temperature, isotopic composition of solvent, concentration of denaturants) can be calculated as prescribed by Englander and co-workers (Bai et al. 1993; Connelly et al. 1993). Only the base-catalyzed exchange is relevant under the current experimental conditions, $\log k_{rc} = \log k_B^{ref} + \log B_L + \log B_R - (\mathrm{pK}_w - \mathrm{pH})$. The reference exchange rate for deuterium-to-proton base-catalyzed exchange in poly-DL-alanine at 20°C was initially taken from Table 1 of (Connelly et al. 1993), $\log k_B^{ref} = 9.87\ \mathrm{M}^{-1}\mathrm{min}^{-1}$.[10] This value was subsequently extrapolated to 5°C, using the activation energy 4 kcal/mol (Bai et al. 1993), $\log k_B^{ref} = 9.71\ \mathrm{M}^{-1}\mathrm{min}^{-1}$. Finally, the correction was introduced to account for the presence of 2 M GdnCl in solution (Loftus et al. 1986), resulting in the value $\log k_B^{ref} = 10.06\ \mathrm{M}^{-1}\mathrm{min}^{-1}$ that was used in the actual calculations.

The terms $\log B_L$ and $\log B_R$, representing the effect of flanking side chains, are tabulated in (Bai et al. 1993). In selecting the values for these parameters we recognize that Asp, Glu, and His side chains are deprotonated under the current experimental conditions; for the P49, S50 pair in drkN SH3 we assume that 12% of the peptidyl-prolyl bond is in the cis conformation (Reimer et al. 1998). To obtain solvent pH, the meter reading has been corrected for the electrode isotope effect (Covington et al. 1968). It is assumed that the correction is linearly dependent on the fraction of D_2O and amounts to 0.2 pH unit in the 50% H_2O–50% D_2O solvent; the corrected pH value used in the computations is 7.7. The ionization constant of water was obtained by linear interpolation between the values from pure H_2O and pure D_2O at 5°C (Covington et al. 1966), $\mathrm{pK_w} = 15.193$. The error associated with the linear approximation is apparently below the uncertainty level of the pH measurement (Gold and Lowe 1967). Finally, to enable the direct comparison with the experiment, the calculated k_{rc} rate should be divided by a factor of 2 to account for the decreased content of H_2O in the 50% H_2O–50% D_2O solvent compared to the reference experiments. As pointed out previously (Mori et al. 1997), the k_{rc} values calculated using this approach are subject to substantial uncertainty.

Acknowledgments We are thankful to Joseph Marsh for helpful discussions. The research has been funded through the NSF grants MCB-044563 and CHE-0723718 to N.R.S.

[10] Note that this constant refers to the deuterium-to-proton exchange catalyzed by OH^-. In the context of our measurement, one is interested in deuterium-to-proton exchange catalyzed by both OH^- and OD^-. The difference, however, appears to be subtle.

References

Bai YW, Milne JS, Mayne L, Englander SW (1993) Primary structure effects on peptide group hydrogen exchange. Proteins Struct Funct Genet 17:75–86

Baxter NJ, Williamson MP (1997) Temperature dependence of ^{1}H chemical shifts in proteins. J Biomol NMR 9:359–369

Best RB, Vendruscolo M (2006) Structural interpretation of hydrogen exchange protection factors in proteins: characterization of the native state fluctuations of CI2. Structure 14:97–106

Bezsonova I, Singer A, Choy WY, Tollinger M, Forman-Kay JD (2005) Structural comparison of the unstable drkN SH3 domain and a stable mutant. Biochemistry 44:15550–15560

Böhlen JM, Rey M, Bodenhausen G (1989) Refocusing with chirped pulses for broadband excitation without phase dispersion. J Magn Reson 84:191–197

Brutscher B, Simorre JP, Caffrey MS, Marion D (1994) Design of a complete set of two-dimensional triple-resonance experiments for assigning labeled proteins. J Magn Reson Ser B 105:77–82

Buck M, Radford SE, Dobson CM (1994) Amide hydrogen exchange in a highly denatured state. Hen egg-white lysozyme in urea. J Mol Biol 237:247–254

Cavanagh J, Rance M (1992) Suppression of cross-relaxation effects in TOCSY spectra via a modified DIPSI-2 mixing sequence. J Magn Reson 96:670–678

Chevelkov V, Faelber K, Diehl A, Heinemann U, Oschkinat H, Reif B (2005) Detection of dynamic water molecules in a microcrystalline sample of the SH3 domain of α-spectrin by MAS solid-state NMR. J Biomol NMR 31:295–310

Chevelkov V, Zhuravleva AV, Xue Y, Reif B, Skrynnikov NR (2007) Combined analysis of ^{15}N relaxation data from solid- and solution-state NMR spectroscopy. J Am Chem Soc 129:12594–12595

Choy WY, Forman-Kay JD (2001) Calculation of ensembles of structures representing the unfolded state of an SH3 domain. J Mol Biol 308:1011–1032

Choy WY, Mulder FAA, Crowhurst KA, Muhandiram DR, Millett IS, Doniach S, Forman-Kay JD, Kay LE (2002) Distribution of molecular size within an unfolded state ensemble using small-angle X-ray scattering and pulse field gradient NMR techniques. J Mol Biol 316:101–112

Connelly GP, Bai YW, Jeng MF, Englander SW (1993) Isotope effects in peptide group hydrogen exchange. Proteins Struct Funct Genet 17:87–92

Covington AK, Robinson RA, Bates RG (1966) Ionization constant of deuterium oxide from 5 to 50 degrees. J Phys Chem 70:3820–3824

Covington AK, Paabo M, Robinson RA, Bates RG (1968) Use of glass electrode in deuterium oxide and relation between standardized pD (pa_d) scale and operational pH in heavy water. Anal Chem 40:700–706

Crowhurst KA, Forman-Kay JD (2003) Aromatic and methyl NOEs highlight hydrophobic clustering in the unfolded state of an SH3 domain. Biochemistry 42:8687–8695

Crowhurst KA, Tollinger M, Forman-Kay JD (2002) Cooperative interactions and a non-native buried Trp in the unfolded state of an SH3 domain. J Mol Biol 322:163–178

Dalvit C (1996) Homonuclear 1D and 2D NMR experiments for the observation of solvent-solute interactions. J Magn Reson B 112:282–288

Dalvit C, Hommel U (1995) Sensitivity-improved detection of protein hydration and its extension to the assignment of fast-exchanging resonances. J Magn Reson B 109:334–338

Delaglio F, Grzesiek S, Vuister GW, Zhu G, Pfeifer J, Bax A (1995) NMRPipe: a multidimensional spectral processing system based on unix pipes. J Biomol NMR 6:277–293

Delepierre M, Dobson CM, Karplus M, Poulsen FM, States DJ, Wedin RE (1987) Electrostatic effects and hydrogen exchange behavior in proteins. The pH dependence of exchange rates in lysozyme. J Mol Biol 197:111–122

Desvaux H, Birlirakis N, Wary C, Berthault P (1995) Study of slow molecular motions in solution using off-resonance irradiation in homonuclear NMR. 2. Fast chemical exchange processes. Mol Phys 86:1059–1073

Dobson CM, Lian L-Y, Redfield C, Topping KD (1986) Measurement of hydrogen exchange rates using 2D NMR spectroscopy. J Magn Reson 69:201–209

Dötsch V, Wider G, Siegal G, Wüthrich K (1995) Interaction of urea with an unfolded protein—the DNA-binding domain of the 434-repressor. FEBS Lett 366:6–10

Eichmüller C, Skrynnikov NR (2005) A new amide proton $R_{1\rho}$ experiment permits accurate characterization of microsecond time-scale conformational exchange. J Biomol NMR 32:281–293

Emsley L, Bodenhausen G (1990) Gaussian pulse cascades—new analytical functions for rectangular selective inversion and in-phase excitation in NMR. Chem Phys Lett 165:469–476

Emsley L, Bodenhausen G (1992) Optimization of shaped selective pulses for NMR using a quaternion description of their overall propagators. J Magn Reson 97:135–148

Englander SW, Poulsen A (1969) Hydrogen-tritium exchange of random chain polypeptide. Biopolymers 7:379–393

Ernst RR, Bodenhausen G, Wokaun A (1987) Principles of nuclear magnetic resonance in one and two dimensions. Oxford University Press, Oxford

Evanics F, Bezsonova I, Marsh J, Kitevski JL, Forman-Kay JD, Prosser RS (2006) Tryptophan solvent exposure in folded and unfolded states of an SH3 domain by ^{19}F and ^{1}H NMR. Biochemistry 45:14120–14128

Farrow NA, Zhang OW, Forman-Kay JD, Kay LE (1994) A heteronuclear correlation experiment for simultaneous determination of ^{15}N longitudinal decay and chemical exchange rates of systems in slow equilibrium. J Biomol NMR 4:727–734

Farrow NA, Zhang OW, Forman-Kay JD, Kay LE (1995) Comparison of the backbone dynamics of a folded and an unfolded SH3 domain existing in equilibrium in aqueous buffer. Biochemistry 34:868–878

Farrow NA, Zhang OW, Forman-Kay JD, Kay LE (1997) Characterization of the backbone dynamics of folded and denatured states of an SH3 domain. Biochemistry 36:2390–2402

Forge V, Wijesinha RT, Balbach J, Brew K, Robinson CV, Redfield C, Dobson CM (1999) Rapid collapse and slow structural reorganisation during the refolding of bovine α-lactalbumin. J Mol Biol 288:673–688

Gal M, Schanda P, Brutscher B, Frydman L (2007) UltraSOFAST HMQC NMR and the repetitive acquisition of 2D protein spectra at Hz rates. J Am Chem Soc 129:1372–1377

Gemmecker G, Jahnke W, Kessler H (1993) Measurement of fast proton exchange rates in isotopically labeled compounds. J Am Chem Soc 115:11620–11621

Gold V, Lowe BM (1967) Measurement of solvent isotope effects with glass electrode. I. The ionic product of D_2O and D_2O-H_2O mixtures. J Chem Soc A:936–943

Griesinger C, Ernst RR (1987) Frequency offset effects and their elimination in NMR rotating-frame cross-relaxation spectroscopy. J Magn Reson 75:261–271

Grzesiek S, Bax A (1992) An efficient experiment for sequential backbone assignment of medium-sized isotopically enriched proteins. J Magn Reson 99:201–207

Grzesiek S, Bax A (1993a) Amino-acid type determination in the sequential assignment procedure of uniformly ^{13}C/^{15}N-enriched proteins. J Biomol NMR 3:185–204

Grzesiek S, Bax A (1993b) The importance of not saturating H_2O in protein NMR: application to sensitivity enhancement and NOE measurements. J Am Chem Soc 115:12593–12594

Hansen PE (2000) Isotope effects on chemical shifts of proteins and peptides. Magn Reson Chem 38:1–10

Harbison GS, Roberts JE, Herzfeld J, Griffin RG (1988) Solid-state NMR detection of proton exchange between the bacteriorhodopsin Schiff-base and bulk water. J Am Chem Soc 110:7221–7223

Hawkes GE, Randall EW, Hull WE, Gattegno D, Conti F (1978) Qualitative aspects of hydrogen-deuterium exchange in ^{1}H, ^{13}C, and ^{15}N nuclear magnetic resonance spectra of viomycin in aqueous solution. Biochemistry 17:3986–3992

Henry GD, Sykes BD (1993) Saturation transfer of exchangeable protons in ^{1}H-decoupled ^{15}N INEPT spectra in water. Application to the measurement of hydrogen exchange rates in amides and proteins. J Magn Reson B 102:193–200

Henry GD, Weiner JH, Sykes BD (1987) Backbone dynamics of a model membrane protein: measurement of individual amide hydrogen exchange rates in detergent-solubilized M13 coat

protein using ^{13}C NMR hydrogen-deuterium isotope shifts. Biochemistry 26:3626–3634

Hitchens TK, McCallum SA, Rule GS (1999) A J^{CH}-modulated 2D (HACACO)NH pulse scheme for quantitative measurement of $^{13}C^{\alpha}$-$^{1}H^{\alpha}$ couplings in ^{15}N, ^{13}C-labeled proteins. J Magn Reson 140:281–284

Hvidt A, Nielsen SO (1966) Hydrogen exchange in proteins. Adv Protein Chem 21:287–386

Hwang TL, Mori S, Shaka AJ, van Zijl PCM (1997) Application of phase-modulated CLEAN chemical EXchange spectroscopy (CLEANEX-PM) to detect water-protein proton exchange and intermolecular NOEs. J Am Chem Soc 119:6203–6204

Hwang TL, van Zijl PCM, Mori S (1998) Accurate quantitation of water-amide proton exchange rates using the Phase-Modulated CLEAN chemical EXchange (CLEANEX-PM) approach with a Fast-HSQC (FHSQC) detection scheme. J Biomol NMR 11: 221–226

Jeener J, Meier BH, Bachmann P, Ernst RR (1979) Investigation of exchange processes by 2-dimensional NMR spectroscopy. J Chem Phys 71:4546–4553

Jensen MR, Kristensen SM, Led JJ (2007) Elimination of spin diffusion effects in saturation transfer experiments: application to hydrogen exchange in proteins. Magn Reson Chem 45:257–261

Kanelis V, Donaldson L, Muhandiram DR, Rotin D, Forman-Kay JD, Kay LE (2000) Sequential assignment of proline-rich regions in proteins: application to modular binding domain complexes. J Biomol NMR 16:253–259

Kateb F, Pelupessy P, Bodenhausen G (2007) Measuring fast hydrogen exchange rates by NMR spectroscopy. J Magn Reson 184:108–113

Kohn JE, Millett IS, Jacob J, Zagrovic B, Dillon TM, Cingel N, Dothager RS, Seifert S, Thiyagarajan P, Sosnick TR, Hasan MZ, Pande VS, Ruczinski I, Doniach S, Plaxco KW (2004) Random-coil behavior and the dimensions of chemically unfolded proteins. Proc Natl Acad Sci USA 101:12491–12496

Koide S, Jahnke W, Wright PE (1995) Measurement of intrinsic exchange rates of amide protons in a ^{15}N-labeled peptide. J Biomol NMR 6:306–312

Kriwacki RW, Hill RB, Flanagan JM, Caradonna JP, Prestegard JH (1993) New NMR methods for the characterization of bound waters in macromolecules. J Am Chem Soc 115:8907–8911

Lesage A, Böckmann A (2003) Water-protein interactions in micro-crystalline Crh measured by ^{1}H–^{13}C solid-state NMR spectroscopy. J Am Chem Soc 125:13336–13337

Lesage A, Gardiennet C, Loquet A, Verel R, Pintacuda G, Emsley L, Meier BH, Böckmann A (2008) Polarization transfer over the water-protein interface in solids. Angew Chem Int Ed 47:5851–5854

Linderstrøm-Lang K (1955) Deuterium exchange between peptides and water. Chem Soc (London) Spec Publ 2:1–20

LiWang AC, Bax A (1996) Equilibrium protium/deuterium fractionation of backbone amides in U-^{13}C/^{15}N labeled human ubiquitin by triple resonance NMR. J Am Chem Soc 118:12864–12865

Loftus D, Gbenle GO, Kim PS, Baldwin RL (1986) Effects of denaturants on amide proton exchange rates: a test for structure in protein fragments and folding intermediates. Biochemistry 25:1428–1436

Marion D, Wüthrich K (1983) Application of phase sensitive two-dimensional correlated spectroscopy (COSY) for measurements of ^{1}H–^{1}H spin-spin coupling constants in proteins. Biochem Biophys Res Commun 113:967–974

Marsh JA, Forman-Kay JD (2009) Structure and disorder in an unfolded state under nondenaturing conditions from ensemble models consistent with a large number of experimental restraints. J Mol Biol 391:359–374

McConnell HM (1958) Reaction rates by nuclear magnetic resonance. J Chem Phys 28:430–431

Melacini G, Kaptein R, Boelens R (1999) Editing of chemical exchange-relayed NOEs in NMR experiments for the observation of protein-water interactions. J Magn Reson 136:214–218

Modig K, Liepinsh E, Otting G, Halle B (2004) Dynamics of protein and peptide hydration. J Am Chem Soc 126:102–114

Mok YK, Elisseeva EL, Davidson AR, Forman-Kay JD (2001) Dramatic stabilization of an SH3 domain by a single substitution: roles of the folded and unfolded states. J Mol Biol 307: 913–928

Mori S, Abeygunawardana C, van Zijl PCM, Berg JM (1996) Water exchange filter with improved sensitivity (WEX II) to study solvent-exchangeable protons. Application to the consensus zinc finger peptide CP-1. J Magn Reson B 110:96–101

Mori S, van Zijl PCM, Shortle D (1997) Measurement of water-amide proton exchange rates in the denatured state of staphylococcal nuclease by a magnetization transfer technique. Proteins Struct Funct Genet 28:325–332

Nishimura C, Dyson HJ, Wright PE (2008) The kinetic and equilibrium molten globule intermediates of apoleghemoglobin differ in structure. J Mol Biol 378:715–725

Otting G, Liepinsh E (1995) Protein hydration viewed by high-resolution NMR spectroscopy: implications for magnetic resonance image contrast. Accounts Chem Res 28:171–177

Otting G, Liepinsh E, Wüthrich K (1991) Protein hydration in aqueous solution. Science 254:974–980

Reimer U, Scherer G, Drewello M, Kruber S, Schutkowski M, Fischer G (1998) Side-chain effects on peptidyl-prolyl cis/trans isomerisation. J Mol Biol 279:449–460

Roder H, Elöve GA, Englander SW (1988) Structural characterization of folding intermediates in cytochrome c by H-exchange labelling and proton NMR. Nature 335:700–704

Schleucher J, Wijmenga SS (2002) How to detect internal motion by homonuclear NMR. J Am Chem Soc 124:5881–5889

Schulman BA, Redfield C, Peng ZY, Dobson CM, Kim PS (1995) Different subdomains are most protected from hydrogen exchange in the molten globule and native states of human α-lactalbumin. J Mol Biol 253:651–657

Shaka AJ, Keeler J, Frenkiel T, Freeman R (1983) An improved sequence for broad-band decoupling: WALTZ-16. J Magn Reson 52:335–338

Shaka AJ, Barker PB, Freeman R (1985) Computer-optimized decoupling scheme for wideband applications and low-level operation. J Magn Reson 64:547–552

Shaka AJ, Lee CJ, Pines A (1988) Iterative schemes for bilinear operators—application to spin decoupling. J Magn Reson 77: 274–293

Shang ZG, Swapna GVT, Rios CB, Montelione GT (1997) Sensitivity enhancement of triple-resonance protein NMR spectra by proton evolution of multiple-quantum coherences using a simultaneous ^{1}H and ^{13}C constant-time evolution period. J Am Chem Soc 119: 9274–9278

Sklenár V, Piotto M, Leppik R, Saudek V (1993) Gradient-tailored water suppression for 1H–15 N HSQC experiments optimized to retain full sensitivity. J Magn Reson A 102:241–245

Skrynnikov NR, Ernst RR (1999) Detection of intermolecular chemical exchange through decorrelation of two-spin order. J Magn Reson 137:276–280

Spera S, Ikura M, Bax A (1991) Measurement of the exchange rates of rapidly exchanging amide protons. Application to the study of calmodulin and its complex with a myosin light chain kinase fragment. J Biomol NMR 1:155–166

Tollinger M, Skrynnikov NR, Mulder FAA, Forman-Kay JD, Kay LE (2001) Slow dynamics in folded and unfolded states of an SH3 domain. J Am Chem Soc 123:11341–11352

Tugarinov V, Choy WY, Kupce E, Kay LE (2004) Addressing the overlap problem in the quantitative analysis of two dimensional NMR spectra: Application to ^{15}N relaxation measurements. J Biomol NMR 30:347–352

van de Ven FJM, Janssen HGJM, Graslund A, Hilbers CW (1988) Chemically relayed nuclear Overhauser effects: connectivities between resonances of nonexchangeable protons and water. J Magn Reson 79:221–235

Vendruscolo M, Paci E, Dobson CM, Karplus M (2003) Rare fluctuations of native proteins sampled by equilibrium hydrogen exchange. J Am Chem Soc 125:15686–15687

Vuister GW, Bax A (1992) Resolution enhancement and spectral editing of uniformly ^{13}C-enriched proteins by homonuclear broadband ^{13}C decoupling. J Magn Reson 98:428–435

Wagner G, Wüthrich K (1982) Amide proton exchange and surface conformation of the basic pancreatic trypsin inhibitor in solution: studies with two-dimensional nuclear magnetic resonance. J Mol Biol 160:343–361

Wang AC, Bax A (1993) Minimizing the effects of radiofrequency heating in multidimensional NMR experiments. J Biomol NMR 3:715–720

Wang AC, Grzesiek S, Tschudin R, Lodi PJ, Bax A (1995) Sequential backbone assignment of isotopically enriched proteins in D_2O by deuterium-decoupled HA(CA)N and HA(CACO)N. J Biomol NMR 5:376–382

Wirmer J, Peti W, Schwalbe H (2006) Motional properties of unfolded ubiquitin: a model for a random coil protein. J Biomol NMR 35:175–186

Xu J, Millet O, Kay LE, Skrynnikov NR (2005) A new spin probe of protein dynamics: nitrogen relaxation in ^{15}N–^{2}H amide groups. J Am Chem Soc 127:3220–3229

Xue Y, Podkorytov IS, Rao DK, Benjamin N, Sun HL, Skrynnikov NR (2009) Paramagnetic relaxation enhancements in unfolded proteins: theory and application to drkN SH3 domain. Protein Sci 18:1401–1424

Yao J, Chung J, Eliezer D, Wright PE, Dyson HJ (2001) NMR structural and dynamic characterization of the acid-unfolded state of apomyoglobin provides insights into the early events in protein folding. Biochemistry 40:3561–3571

Zangger K, Armitage IM (1998) Sensitivity-enhanced detection of fast exchanging protons by an exchange-edited gradient HEHA-HA-HSQC experiment. J Magn Reson 135:70–75

Zhang OW, Forman-Kay JD (1997) NMR studies of unfolded states of an SH3 domain in aqueous solution and denaturing conditions. Biochemistry 36:3959–3970

Zhang OW, Kay LE, Olivier JP, Forman-Kay JD (1994) Backbone ^{1}H and ^{15}N resonance assignments of the N-terminal SH3 domain of drk in folded and unfolded states using enhanced-sensitivity pulsed-field gradient NMR techniques. J Biomol NMR 4: 845–858

Zheng ZW, Gryk MR, Finucane MD, Jardetzky O (1995) Investigation of protein amide-proton exchange by ^{1}H longitudinal spin relaxation. J Magn Reson B 108:220–234

Zhou JY, van Zijl PCM (2006) Chemical exchange saturation transfer imaging and spectroscopy. Prog NMR Spectrosc 48:109–136